**Infinite Science Publishing**

*Proceedings Article*

# Automated MPI segmentation in X-space and calibration to quantify iron concentration in a tracer distribution

Zewen Sun[a,b] · Jie Tian[a,c] · Yang Du[a,b,*]

[a]CAS Key Laboratory of Molecular Imaging, the State Key Laboratory of Management and Control for Complex Systems, Institute of Automation, Chinese Academy of Sciences, Beijing, China
[b]School of Artificial Intelligence, The University of Chinese Academy of Sciences, Beijing, China
[c]Beijing Advanced Innovation Center for Big Data-Based Precision Medicine, School of Medicine Science and Engineering, Beihang University, Beijing, China
*Corresponding author, email: yang.du@ia.ac.cn

## Abstract

Magnetic particle imaging (MPI) is a new, radiation-free medical imaging modality that relies on the non-linear magnetization response of superparamagnetic iron oxide nanoparticles (SPIONs) to reconstruct their concentration distribution with high sensitivity and medical safety. Current quantification methods for region of interest (ROI) are inadequate and are usually outlined manually or using deep learning methods. We propose two new models for ROI selection based on machine learning, one is the K-means++-based threshold-inflated image segmentation model and the other is the image segmentation model based on MPI simulation and SVM. We have developed an accurate quantification of 2D MPI images and established the calibration curve to predict the corresponding iron content based on the MPI image.

## I. Introduction

Magnetic particle imaging (MPI) is a novel radiation-free medical imaging modality that can directly image the spatial concentration distribution of superparamagnetic iron oxide nanoparticles (SPIONs) tracers [1] with high sensitivity [2] and independent from tissue depth-dependent characteristics. Compared to clinical magnetic resonance imaging (MRI), MPI has the advantage of positive contrast imaging [3]. Preclinical studies have demonstrated the great potential of MPI in biomedical applications such as stem cell tracking [4], cancer imaging [5], intestinal bleeding detection [6], lung imaging [7][8], and stroke detection [9].

Currently we often outline the region of interest (ROI) i.e., the region with tracer material in the MPI image manually, which leads to low efficiency and the results are subjectively affected by the operators. Deep learning algorithms such as convolutional neural networks have potential but have many limitations like requiring large amounts of labeled data for training the neural network [10]. However, machine learning algorithms such as unsupervised learning algorithms based on clustering, can be optimized for a wide range of data, and supervised learning algorithms such as support vector machines (SVM) show many unique advantages in solving small sample, non-linear and high-dimensional pattern recognition.

We propose two new models for ROI selection, the K-means++-based threshold-inflated image segmentation model and the image segmentation model based on MPI simulation and SVM. To evaluate the effectiveness of them for the quantitative analysis of 2D MPI images, two experiments are designed in this work.
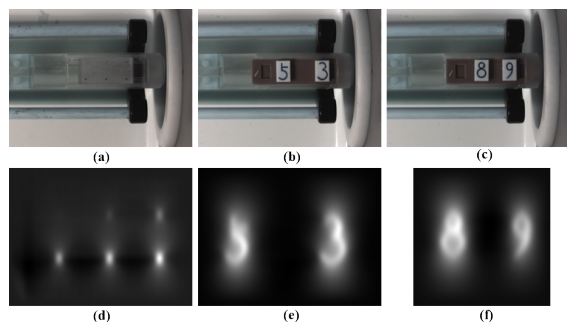
**Figure 1:** (a) Calibration phantom, (b) phantom "5" and "3", (c) phantom "8" and "9", (d) the MPI image of calibration phantom, (e) the MPI image of phantom "5" and "3", (f) the MPI image of phantom "8" and "9".

This work provides a mechanism that allows accurate selection of ROI from 2D MPI images and subsequent analysis of ROI to achieve prediction of the corresponding iron content based on the MPI image.

## II. Material and methods

### II.I. 3D-Printed Phantom Preparation and MPI Protocol

Five 3D-printed constructs were generated—a calibration phantom containing six small cubes, a "5", a "3", a "8" and a "9" phantom. SPION solutions (synomag®-D, Micromod) of various concentrations were prepared. Six small cubes of the calibration phantom were filled with six concentrations of tracer, 2.5 µg/µL, 2.0 µg/µL, 1.5 µg/µL, 1.0 µg/µL, 0.5 µg/µL, and 0.25 µg/µL, respectively. Other phantoms were injected with tracer at a concentration of 1 µg/µL. The total iron value (TIV) was recorded for validating and comparing the prediction of the proposed algorithms to the actual TIV injected into the constructs. The parameters such as field of view (FOV), gradient of selection field, excitation frequency, and scanning trajectory were important for the imaging quality. Based on the x-space reconstruction algorithm, we acquired the simulated MPI images by setting the scanning parameters consistent with the commercial machine: a 4cm×6cm FOV, a 5.7 T/m selection field gradient, a drive field strength of 20 mT peak amplitude and a 45.0 kHz drive frequency. We set the diameter of the particles for scanning to 50 nm and the environmental temperature to 293 K. Finally, we obtained the simulated images, which had a pixel resolution of 0.25 mm. Phantoms were scanned by MPI device MOMENTUM imager (Magnetic Insight, Inc., Alameda, CA) using the default scan mode, which had a moderate sensitivity, resolution and acquisition time. The 3D printed phantoms and their corresponding 2D MPI images are shown in Fig.1.

### II.II. K-means++-based Threshold-inflated Image Segmentation Model

We propose a K-means++ based threshold-inflated image segmentation algorithm to select the ROI of MPI images. The algorithm flow is as follows.

1. Setting a threshold value to segment the MPI image and pixel values below this threshold are set to 0 and pixel values above the threshold remain unchanged, resulting in segmentation of the MPI foreground and background images.

2. Clustering of pixel locations in the foreground MPI image using the K-means++ algorithm [11], which in this work uses the elbow rule to determine the k value, resulting in k classes.

3. Finding the pixel point with the largest pixel value in each cluster and using it as the starting point for threshold inflation, the object of the threshold inflation operation is the original MPI image. This is done by first setting a threshold and then visiting the 4-neighbourhood pixel points of this pixel point, adding them to the visited list if the pixel value is above the threshold and leaving them unprocessed if the pixel value is below the threshold.

4. Continuing the threshold inflation operation for new pixel points added to the visited list until the visited list no longer changes.

5. The pixel points in the visited list are merged and the final segmented image is output.

### II.III. Image Segmentation Model Based on MPI simulation and SVM

We propose a new image segmentation model based on the MPI simulation and SVM. We utilized a flexible and easy-to-use MPI reconstruction framework (MPIRF) [12], which integrates the x-space [13] and system matrix methods for scan simulation and image reconstruction and can simulate the working process of MPI scanners. The trained SVM can classify each pixel in the image to achieve ROI selection. The training dataset was produced using MPIRF. Handwritten digital images of 0-9 in the MNIST handwriting dataset and a square image were used as the phantom images, as shown in Fig.2(a)-(k). Their corresponding MPI images are shown in Fig.2(l)-(v). A sub-image of size 50 × 50 is intercepted in the center of the MPI image of 0-9 and the upper left corner of the MPI image of the small square as the training data set, and the size of the training data set i.e., the number of pixels is 27500.
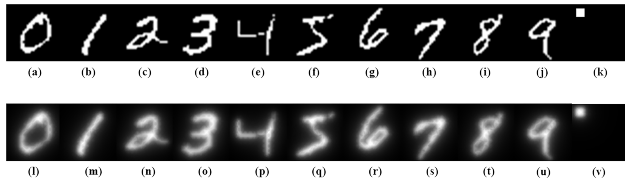
**Figure 2:** (a)-(k) The phantom images, (l)-(v) the corresponding MPI images.
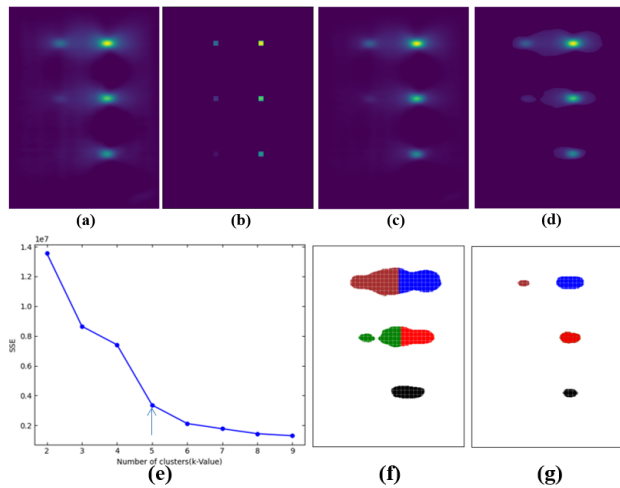


**Figure 3:** (a) The original image, (b) the ground truth, (c) the gamma-corrected image, (d) foreground signals, (e) elbow method graph indicating SSE (sum squares of error) per selected k value, (f) clustering results, (g) segmented ROI obtained using the K-means++ based threshold-inflated image segmentation model.



**Figure 4:** The linear relationship between MPI signal and iron concentration.



**Figure 5:** Calibration curve.

# III. Results and discussion

## III.I. Calibration Curve Establishment

In this experiment, the calibration curve was established. Fig.3 shows the result of the K-means++ based threshold-inflated image segmentation model. Each color indicates a class in Fig.3(f)&(g). The final segmented ROI contains four parts, and two parts were lost during the image processing. The MPI signal here means the pixel value in the MPI image.

The unit pixel MPI signal and unit pixel iron concentration are calculated for the six phantom regions in the ground truth and then linearly regressed in least squares. The result are shown in Fig.4. The linear relationship is y=0.0001x+0.0015, $R^2$=0.9952. This linear relationship was used to calculate the iron content and MPI signal in reconstructed signal intensity of the four ROIs separately. Linear regression was performed on the MPI signal and the iron content, and the result is shown in Fig.5. The calibration curve is y=0.0001x+0.0479, $R^2$=0.9999.
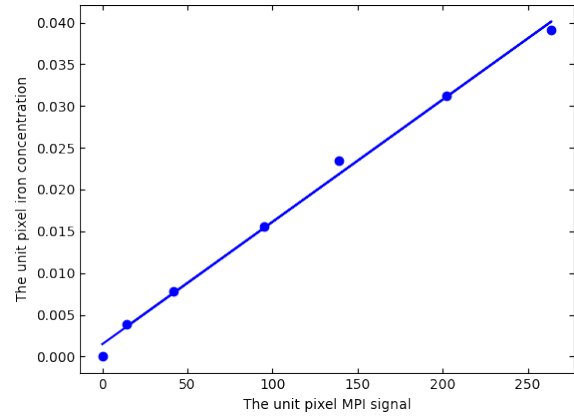
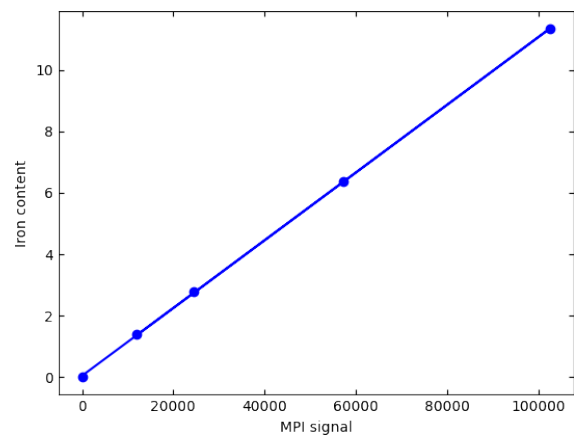## III.II. Accuracy Verification of Calibration Curve

The K-means++-based threshold-inflated image segmentation model is first applied to MPI images of phantom "5", "3", "8" and "9", and the result can be seen in Fig.6(b)&(e). Then the image segmentation model based on MPI simulation and SVM is applied, and the segmented ROI shown in Fig.6(c)&(f). The total MPI signals of ROI and the corresponding TIV are shown in Table 1. The first three relative errors are 0.04%, 0.02% and 0.26% indicating that the accuracy of the calibration curve is high, and the model segmented the ROI well. The worst result for phantom "9" is just a segmentation error of the phantom, which can always happen. The other phantoms are quite well separated and the predicted TIV are quite accurate.

# IV. Conclusions

We propose two new models for ROI selection, the K-means++-based threshold-inflated image segmentation
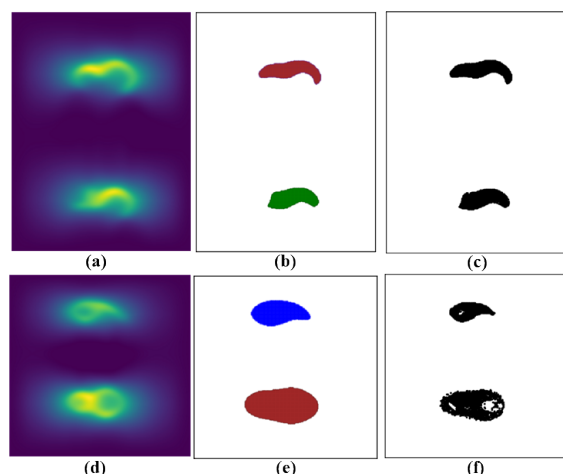
**Figure 6:** (a) & (d) The original MPI image, (b) & (e) the corresponding initial segmented ROI, (c) & (f) the corresponding final segmented ROI obtained using the image segmentation model based on MPI simulation and SVM.

**Table 1:** TIV information.

| phantom | actual TIV (µg) | predicted TIV (µg) | relative error |
|---------|-----------------|--------------------|----------------|
| 5       | 166.18          | 166.10640          | 0.04%          |
| 3       | 190.34          | 190.38518          | 0.02%          |
| 8       | 244.98          | 245.62478          | 0.26%          |
| 9       | 165.54          | 127.97111          | 22.70%         |

model and the image segmentation model based on MPI simulation and SVM. Experiments have shown that our methods can segment the MPI images accurately and we have completed quantification by obtaining the calibration curve so that the corresponding iron content can be known from the MPI image.

## Acknowledgments

## Author's statement

Authors state no conflict of interest. Informed consent has been obtained from all individuals included in this study.

## References

[1] Gleich B, Weizenecker R. Tomographic imaging using the nonlinear response of magnetic particles. Nature,2005, 435(7046): 1214-1217.

[2] Zhi W T, Hensley D W, Chandrasekharan P, et al. Optimization of drive parameters for resolution, sensitivity and safety in magnetic particle imaging. IEEE Transactions on Medical Imaging, 2020, 39(5): 1724-1734.

[3] Knopp T, Gdaniec N, Möddel M. Magnetic particle imaging: from proof of principle to preclinical applications. Physics in Medicine & Biology, 2017, 62(14): R124.

[4] Zheng B, von See M P, Yu E, et al. Quantitative magnetic particle imaging monitors the transplantation, biodistribution, and clearance of stem cells in vivo. Theranostics, 2016, 6(3): 291.

[5] Yu E Y, Bishop M, Zheng B, et al. Magnetic particle imaging: a novel in vivo imaging platform for cancer detection. Nano Letters, 2017, 17(3): 1648.

[6] Yu E Y, Chandrasekharan P, Berzon R, et al. Magnetic particle imaging for highly sensitive, quantitative and safe in vivo gut bleed detection in a murine model. Acs Nano, 2017: acsnano.7b04844.

[7] Wei T Z, Prashant C, Yedda Z X, et al. In vivo tracking and quantification of inhaled aerosol using magnetic particle imaging towards inhaled therapeutic monitoring. Theranostics, 2018, 8(13): 3676-3687.

[8] Xinyi, Y, Zhou, et al. First in vivo magnetic particle imaging of lung perfusion in rats. Physics in Medicine & Biology, 2017.

[9] Ludewig P, Gdaniec N, Sedlacik J, et al. Magnetic particle imaging for real-time perfusion imaging in acute stroke. ACS nano, 2017, 11(10): 10480-10488.

[10] Thrall J H, Li X, Li Q, et al. Artificial intelligence and machine learning in radiology: opportunities, challenges, pitfalls, and criteria for success. Journal of the American College of Radiology, 2018, 15(3): 504-508.

[11] Hayat H, Sun A, et al. Artificial intelligence analysis of magnetic particle imaging for islet transplantation in a mouse model. Molecular imaging and biology, 2021, 23: 18-29.

[12] Shen Y, Hu C, Zhang P, Tian J, Hui H. A novel software framework for magnetic particle imaging reconstruction. Int J Imaging Syst Technol. 2022; 1-14.

[13] Goodwill P W, Conolly S M. The X-space formulation of the magnetic particle imaging process: 1-D signal, resolution, bandwidth, SNR, SAR, and magnetostimulation. IEEE Trans Med Imaging. 2010; 29(11): 1851-1859.